Exploratory Passive Control Study of a Supersonic Multi-Stream Nozzle Flow

Emma D. Gist[*,a], Parshwanath S. Doshi[*,b], Seth W. Kelly[*,a], Mark N. Glauser[†,a], Datta V. Gaitonde[†,b]

Mechanical and Aerospace Engineering

[a]Syracuse University
Syracuse, NY

[b]The Ohio State University
Columbus, OH

Large Eddy Simulations (LES) and experimental measurements are performed to examine different aspects of a supersonic multi-stream jet representing a canonical airframe-integrated variable cycle engine architecture. The flowfield consists of two streams separated by a splitter plate; an upper supersonic core stream (Mach = 1.6) and a lower bypass stream (Mach = 1), which exit onto an aft-deck plate. Previous experimental and numerical efforts have shown that an instability associated with the splitter plate trailing edge exhibits a global influence on the flow because of its interaction with the shock train. The instability is also responsible for impairing the effectiveness of the bypass stream as a thermal and acoustic barrier between the core jet and the airframe. In the first part of this study, the potential for passive flow control by introducing sinusoidal spanwise modifications along the splitter plate edge is explored. The underlying mechanisms are explored computationally using LES on a simplified configuration that isolates the splitter plate. Results on two different spanwise wave numbers indicate that the sinusoidal trailing edge induces streamwise vorticity, which enhances mixing between the two streams and breaks up the shed structures seen previously. The tone is suppressed, together with small changes in the mean shock locations and shear layer trajectories. These spanwise modifications are in the process of being tested in the experimental facility using the full multi-stream nozzle. In a complementary effort, geometric modifications to the aft-deck and its effects on the flowfield are examined experimentally using the actual test rig. Results on the nominal deck length are compared with those from a half and double length deck, and without the deck. In each case, the shock train initiated at the SERN persists, and influences the downstream plume development. Although the impact on the tone is relatively small, the plume itself shows perceptible change. The extended deck results in a small downward movement of the plume relative to the nominal length, while the half nominal length displays larger spread of the lower shear layer initiated at the deck edge. Current efforts are focused on using the results to target complementary simulations and experiments for each tested modification.

I. Nomenclature

β	=	Spanwise wavenumber
ρ	=	Density
P	=	Pressure
T	=	Temperature
t	=	Time
M_∞	=	Freestream Mach Number
Re	=	Reynolds Number
LES	=	Large Eddy Simulation
$SPTE$	=	Splitter Plate Trailing Edge
PSD	=	Power Spectral Density
POD	=	Proper Orthogonal Decomposition
$SPOD$	=	Spectral Proper Orthogonal Decomposition
PIV	=	Particle Image Velocimetry

[*]PhD Student
[†]Professor, AIAA Fellow

LDA = Laser Doppler Anemometry
NPR = Nozzle Pressure Ratio
$SERN$ = Single Expansion Ramp Nozzle
$MARS$ = Multi-Aperture Rectangular SERN
$SBLI$ = Shockwave Boundary Layer Interactions
D_h = Hydraulic Diameter
h_e = Nozzle exit height
w = Nozzle width
V = Velocity vector

II. Introduction

ENGINE flowpath design continues to be dictated by the need to improve various aircraft capabilities, such as speed, fuel economy, engine and airframe noise [1], environmental impact and mechanical reliability [2]. For this reason, the jet engine has undergone several modifications since its original design[3]. These changes have included the incorporation of materials with better properties, afterburners, and fans with bypass streams to enhance propulsive efficiency at different speeds of operation [4].

The variable cycle engine discussed by Simmons [5] (see Fig.1) is an example of a modern design, with some additional features such as a Single Expansion Ramp Nozzle (SERN) and an additional bypass stream. These characteristics accrue several advantages, including better airframe integration, lower pressure drag compared to axisymmetric nozzles [6], the ability to incorporate thrust-vectoring [7] and to switch between high specific thrust and high fuel economy modes of operation, depending on flight requirements [5].

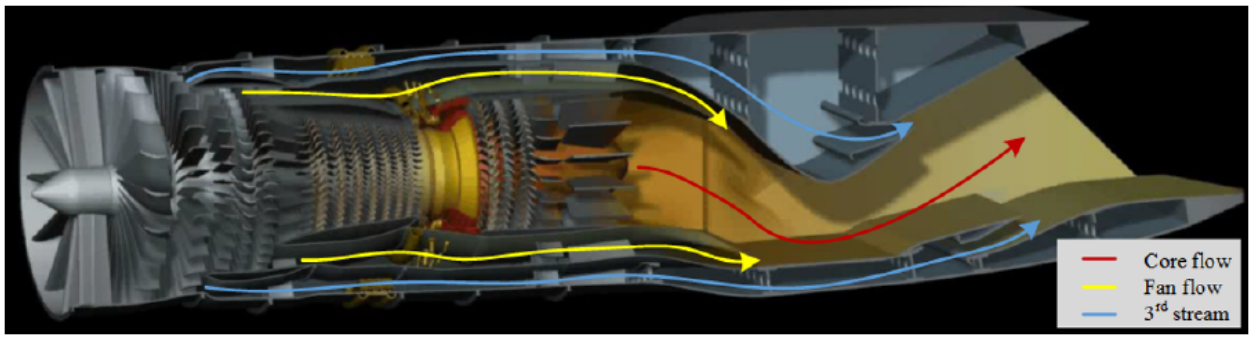

Fig. 1 Variable Cycle Engine studied by Simmons [5].

The inclusion of the secondary bypass stream, referred to as the lower or deck stream in this paper, affords the design engineer a number of potential benefits other than improving the operating efficiency. It can shield the deck from the thermal loading of the core stream [8], decrease noise [9–11] and reduce spillage drag for supersonic aircraft at part power [12]. The configuration, designated Multi-Aperture Rectangular SERN (MARS), is shown in Fig. 2, while a canonical extension is shown in Fig. 3. The principal components are identified as the SERN, the splitter plate that separates the deck from the core stream and the deck itself. The nozzle flowfield is complicated by the presence of supersonic waves, shock-wave boundary layer interactions (SBLI), mixing layers, turbulence, multiple boundary layers, and the finite spanwise extent of the geometry.

The results of extensive experimental campaigns, using a variety of advanced diagnostics, have been described by Berry *et al.* [13–16] and Magstadt *et al.* [10, 17]. Concurrently, high-fidelity Large-Eddy Simulations (LES) at the same conditions have been performed by Stack & Gaitonde [18, 19]. These efforts have jointly elucidated the key features of the flowfield encountered in this configuration.

An example is shown using a time-averaged $\tilde{V} \cdot \nabla P$ plot from [19] in Fig. 4 to visualize the shock structure in the flow. The core stream is supersonic (Ma = 1.6) while the deck stream is sonic (Ma = 1). At design operating conditions, the above studies have shown that the effectiveness of the deck (or third) stream can be compromised by phenomena arising due to the interaction of the mixed core and first bypass streams (referred to as simply the upper or core stream in this paper). Specifically, a vortex shedding instability arises downstream of the edge of the splitter plate separating the

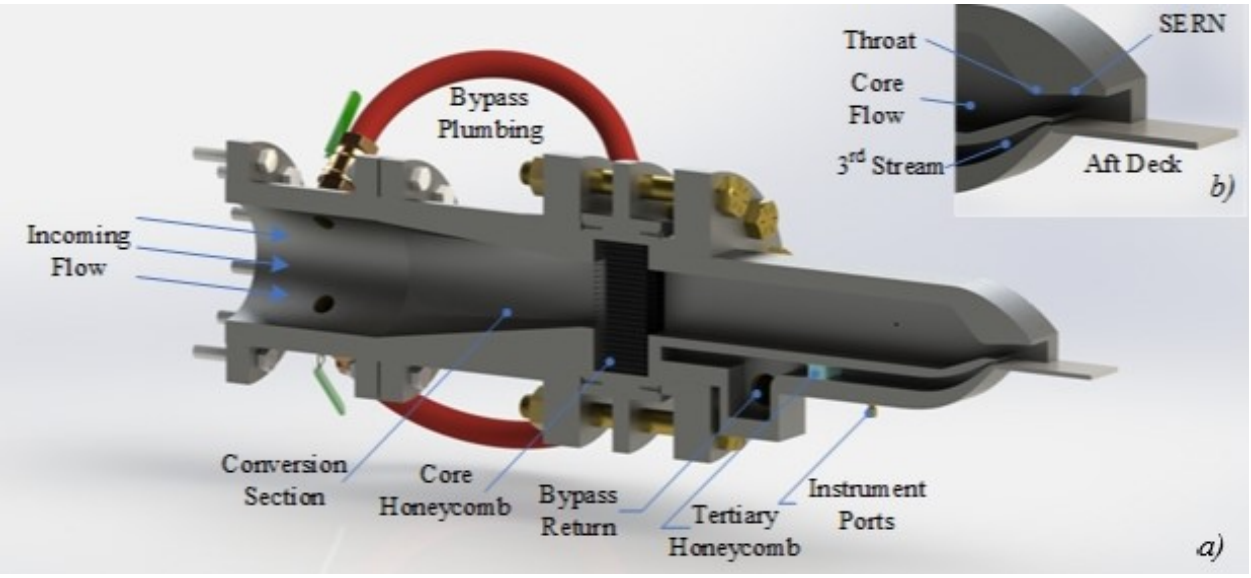

Fig. 2 Cross-Sectional CAD rendering of the MARS jet rig [13].

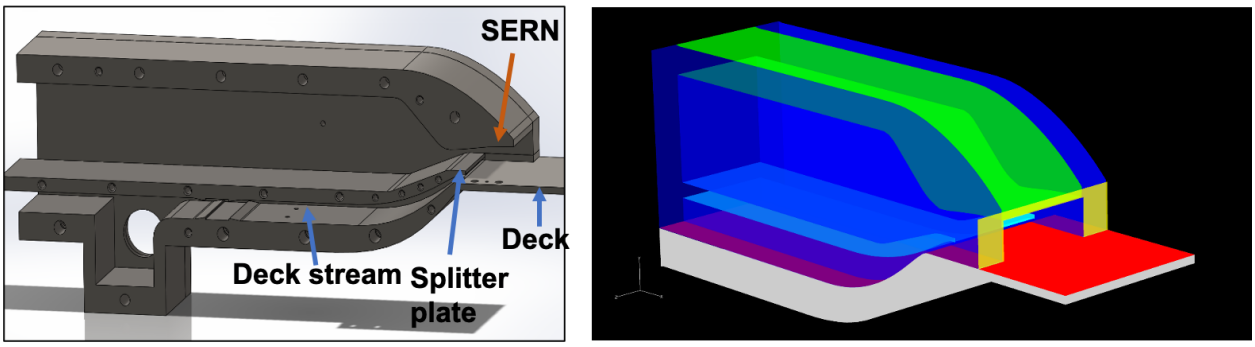

Fig. 3 Canonical configuration showing experimental design (left) and simulation model (right)

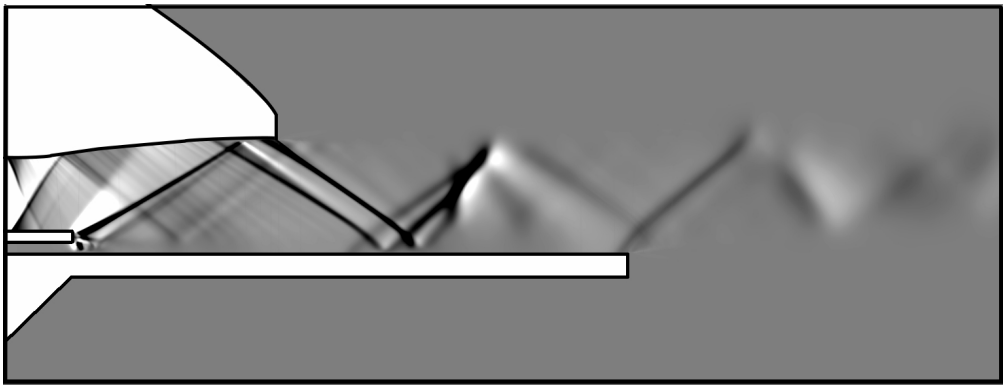

Fig. 4 Streamwise plot of $\vec{V} \cdot \nabla P$ taken from [19]. The black lines indicate compression waves and shocks, while the white lines indicate expansion waves.

two streams. The influence of this instability is observed in the entire flowfield, with special concern arising due the imposed unsteady loading on the deck and the acoustic signature in the farfield.

Since the origins of this instability are associated with the splitter plate trailing edge (SPTE), this region is identified

as a particularly sensitive region of the flow and lends itself to being a prime candidate for applying flow control [19, 20]. The dynamics of the vortex-shedding at the SPTE have been discussed by the cited references. A recent computational effort by Stack & Gaitonde [21] summarizes the observations. The shedding from the splitter plate is different from the more traditionally examined symmetric counterpart described by Gerrard [22] in which the freestream conditions are the same on either side of the body. In the present flow, the asymmetry in the freestream conditions above and below the splitter plate affects the growth rate and trajectory of the shear layers. This can result in a downward deflection of the overall mixing layer towards the deck, where the flow then interacts with the deck boundary layer. This deflection, coupled with other aspects of the geometry and the supersonic nature of the core stream, sets up a series of shock trains and expansion waves that reflect off the SERN, the deck plate, and the shear layers near the exit. Additionally, the vortex forming on the deck stream side is observed to have a shorter lifespan than that forming on the core stream side, due to the dissipative effects of the deck surface. Only the core stream vortex is able to propagate farther into the flow and interact with the first shock in the primary shock train, which then carries the unsteadiness forward and affects the rest of the flow. This affects the observed frequency signature in the rest of the flow, which is a subharmonic of the initiating phenomenon, since one of every two shed vortices is effectively destroyed [19]. SPOD and deck surface pressure spectra also revealed that the splitter plate unsteadiness was closely related to the deck surface pressure unsteadiness, further demonstrating the need for controlling the shedding at the SPTE.

The overall goal of this paper is to examine flow control; presently the focus is on passive approaches. The present study is a part of an ongoing collaborative effort between experiments at Syracuse University's Skytop Turbulence Laboratory and numerical studies at The Ohio State University's High Fidelity Computational Multi-Physics Group. In prior efforts (see *e.g.,* Ref. [14]), the fusion of experiments and simulations was performed through the development of model-order reduction efforts that leverage the long time-traces available for the former with the high time-accuracy of the latter. The present work continues this joint effort by effectively performing experimental and simulation campaigns in a complementary manner. In the present paper, we address different but related aspects of the same problem independently, as a first step towards generating a unified view of possible methods of control. Specifically, measurements and calculations are performed on two broad strategies as described below, to develop a fundamental understanding as well as to ensure the feasibility of proposed approaches.

One obvious choice is to alter the geometry of the splitter plate, since it is the origin of the most dominant instabilities. Evidence to support this observation may be derived for example from the work of Ruscher *et al.* [20], who performed LES studies of two splitter plate configurations, one with a flat plate and the other with a knife-edge shaped plate. This introduced the deck stream at an angle rather than parallel to the core flow. They observed that the shedding from the plate edge ceased in the knife-edge case, with the primary instability morphing into a Kelvin-Helmholtz instability. This dramatic change also affected the rest of the shock-train development and reduced mixing between the two streams. Stack [19] explored the effects of different splitter plate thicknesses (one-half and one-tenth of the original thickness) on the instability of the mixing layer. Similar to Rusher *et al.* [20], it was observed that a decrease in the splitter plate thickness at the trailing edge changes the dominant instability mechanism from absolute to convective. POD on the different cases reveals that there is also a large difference in the energy content of the structures in the two different types of instabilities, with the shedding instability structures containing nearly 50% of the energy, while the Kelvin-Helmholtz structures contain about 16%. Although thinning out the SPTE as a means for achieving flow control appears promising, such a solution has detrimental structural implications.

Trailing edge devices are a natural choice to examine flow control. For a canonical mixing layer, Fernando & Menon [23] experimentally examined the effects of different SPTE geometries on the degree of mixing between the two streams of a mixing layer configuration. They introduced three-dimensional trailing-edge devices in a periodic fashion, with the hypothesis that this would create streamwise vorticity and hence promote mixing. They observed however, that the devices substantially enhanced the mixing but only on the lower Mach number side of the flow.

Lewalle *et al* [24], in the processing of LES data provided by Stack [25], examined the convection of structures in the wake of the splitter plate. Isosurfaces of vorticity shed from the SPTE region appear to have a distinct spanwise wavelength. These isosurfaces exhibit significant curvature, with coherence in the streamwise direction *i.e.,* the spanwise structure does not break down rapidly downstream, as may be expected due to turbulence. Whether this is essentially the dominance of convection or is caused by some other mechanism remains to be determined. However, the presence of a prominent spanwise wavelength serves as motivation for this investigation to employ passive control to the highly receptive region to excite this instability. In this paper, initial simulation efforts, employed as a means to provide guidance to an ongoing experimental campaign, are described.

A second approach of current interest, also passive in nature, is to alter the response of the aft-deck, which essentially simulates the integration of the nozzle into an airframe. Effects of geometric modifications of the aft-deck length have

been described by Berry [16], who characterized the flow field for a no-deck, a half-nominal deck, and nominal deck configuration. The presence of an aft-deck extending outward from the jet nozzle was shown to influence the growth of the shear layers and the deflection of the jet plume. Furthermore, elongating the deck to the nominal length provided a more organized shock structure. The work of [16] is continued in this study where an additional deck plate, twice the nominal length, is surveyed experimentally.

In Section III, the effect of introducing a spanwise undulation in the SPTE is discussed using LES to provide an initial assessment for the ongoing experimental effort. The numerical setup is discussed in Section III.A, which includes the governing equations, boundary conditions, grid features and numerical schemes, while unsteady and mean results on two non-zero *beta* cases are discussed in Section III.B. The effect of the aft-deck length is examined in Section IV, which includes a discussion of the diagnostics (Section IV.A) and initial results on the velocity field and spectral response (Section IV.B). Section V provides a summary and delineates an outline for future work.

III. Wavy Splitter Plate Trailing Edge

In the present work, we seek to build upon the work of Stack and Gaitonde [21], Ruscher *et al* [20] and Lewalle *et al* [24] to investigate the effect of sinusoidal spanwise modifications to the SPTE geometry with the overall goal of reducing the observed tone. In particular, we consider the effects of a non-zero spanwise SPTE wavenumber on the dynamics of a simple canonical mixing layer, the freestream conditions and plate thickness of which match those of the complete nozzle configurations studied by Stack [19] and Magstadt *et al* [17].

A. Numerical Setup

Three different SPTE configurations have been considered in this study: a straight edge ($\beta = 0$), a $\beta = 0.8$, and a $\beta = 1.2$, using the setup shown in Fig. 5. The LES results were obtained by solving the full 3D nondimensionalized

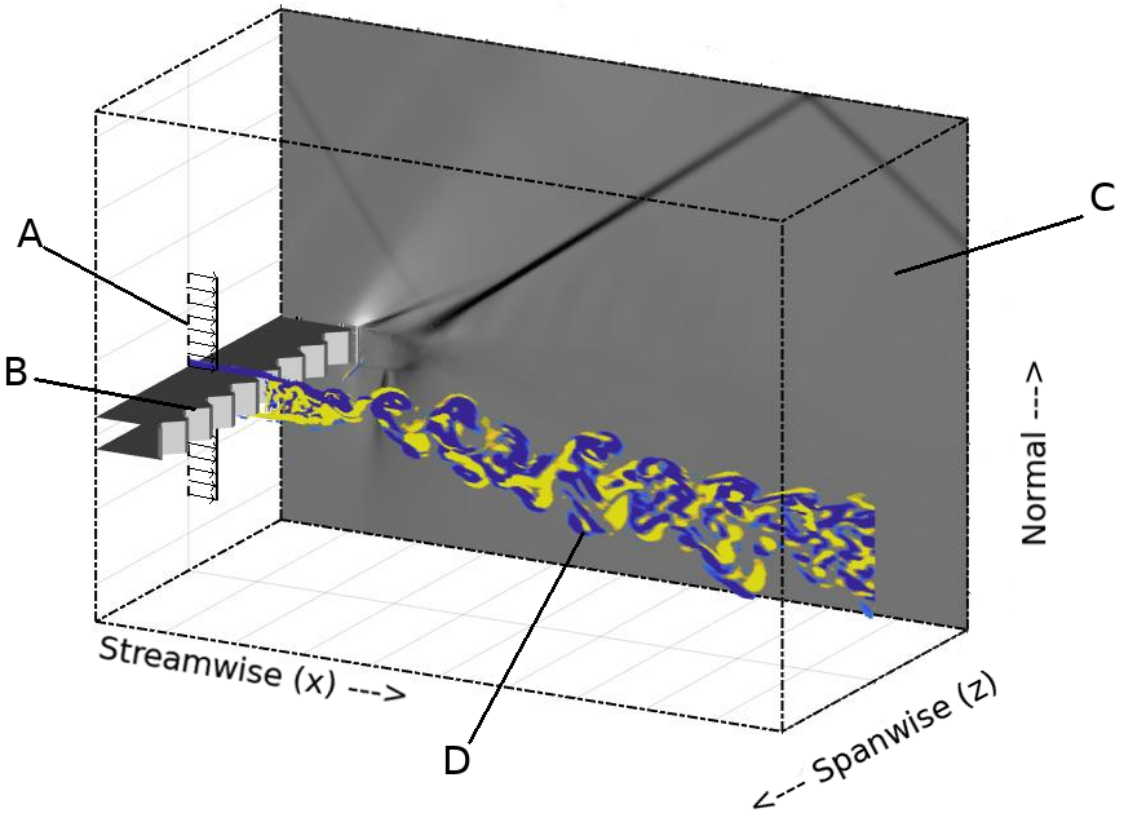

Fig. 5 Schematic of the LES setup. A) The incoming turbulent boundary layer B) The trailing edge of the splitter plate C) A time-averaged numerial Schlieren ($\frac{\partial \rho}{\partial x}$) D) An instantaneous snapshot of the shear layer, visualized using the spanwise vortcity

compressible Navier-Stokes equations in strong conservation form on a curvilinear mesh:

$$\frac{\partial}{\partial \tau}\left(\frac{U}{J}\right) + \frac{\partial F}{\partial \xi} + \frac{\partial G}{\partial \eta} + \frac{\partial H}{\partial \zeta} = \frac{1}{Re}\left[\frac{\partial F_v}{\partial \xi} + \frac{\partial G_v}{\partial \eta} + \frac{\partial H_v}{\partial \zeta}\right] \tag{1}$$

where the variable vector U consists of the conserved variables, F,G,H represent inviscid fluxes and F_v,G_v,H_v represent the viscous fluxes respectively. J is the Jacobian determinant of the transformation that relates the Cartesian (x,y,z) coordinate system to the curvilinear (ξ,η,ζ) system. The molecular viscosity is modeled using Sutherland's law:

$$\mu = T^{3/2}\left(\frac{1 + S/T_{ref}}{T + S/T_{ref}}\right) \tag{2}$$

with T_{ref} being the reference temperature used in the nondimensionalization and S = 110.4K being Sutherland's temperature. The second coefficient of viscosity λ is based on Stokes' hypothesis ($\lambda = -2/3\mu$) and the equation of state in nondimensional form is used to relate pressure with density and temperature,

$$P = \frac{1}{\gamma M_\infty^2}\rho T \tag{3}$$

The governing equations above are nondimensionalized using a length scale based on the thickness of the splitter plate (3.175mm) in the original setup studied by [17]. The reference velocity (u_{ref}) and density (ρ_{ref}) are based on the average streamwise velocity and density of the upper and lower streams, and are equal to $327m/s$ and $1.89kg/m^3$. The reference molecular viscosity was obtained using Sutherland's law (Eqn.2) and a reference temperature based on the average of the two freestream temperatures, while pressure was nondimensionalized using $P_{ref} = \rho_{ref}u_{ref}^2$.

The schematic in Fig.5 shows the primary features of the numerical domain. The freestream conditions on either side of the plate are modeled to isolate the conditions in the full nozzle configuration (Fig.4). Thus, the upper stream is at M_∞ = 1.23 while the bottom stream is at M_∞ = 1. No-slip and adiabatic boundary conditions are applied on the surface of the splitter plate. The top boundary is modeled as an inviscid wall to allow shock reflections and simulate the confinement aspect of the actual nozzle. The location above the plate is the same as that between the SERN and the plate in the full configuration. The lower computational boundary is set to freestream conditions of the lower stream. The spanwise boundaries are periodic, while the downstream boundary is set to a zero-gradient condition. Simulating the complete laminar to turbulent boundary layer transition at the inlet of the domain is computationally prohibitive; thus the inflow turbulence is independently specified using the digital filtering method described by [26].

Since the characteristics of the splitter plate trailing edge and the flow immediately downstream of it are of primary interest in this study, the size of the domain is selected to ensure that the farfield boundaries are sufficiently far away from the splitter plate surface. The spanwise extent of the geometry is chosen to be 10 times the splitter plate thickness, so as to be able to simulate a sufficient number of spanwise wavelengths and allow the growth of larger spanwise instabilities than the spanwise wavenumber, if they exist. Grid-stretching is incorporated near the open boundaries to allow for numerical dissipation of disturbances that might reflect off them. The simulations were performed on a 3D mesh with 476 points along the streamwise, 557 points along the normal and 235 points along the spanwise direction. Care was taken to ensure that the sinusoidal features of the SPTE in the non-zero β cases were adequately resolved. For these cases, the number of points used to resolve each crest and trough was always greater than 20. The amplitude of the crests and troughs was fixed at 0.25 times the thickness of the splitter plate.

The inviscid fluxes were discretized using an upwind biased Roe scheme [27] with third-order MUSCL reconstruction and a Van Leer harmonic limiter [28]. Time-marching was done using an implicit Beam-Warming scheme with two sub-iterations and approximate factorization. The non-dimensional time-step size for the simulations was fixed at $5e^{-4}$ which amounts to a physical time-step size of approximately 48 nanoseconds.

B. Results

The effect of the spanwise sinusoidal variations on the SPTE are easily apparent in the isosurfaces of Q-criterion, colored by streamwise velocity, as shown in Fig.7. In the straight edge case, the isosurfaces resemble classical roller structures forming off the SPTE, indicative of the predominant spanwise vorticity, which is the primary component in the boundary layers developing on either side of the splitter plate. The braid region between the rollers contain the well known rib structures. As noted earlier, the characteristics of the instability are more complicated than the traditional case of equal streams on either side of the plate; in the present case, the wake is modulated by the velocity difference

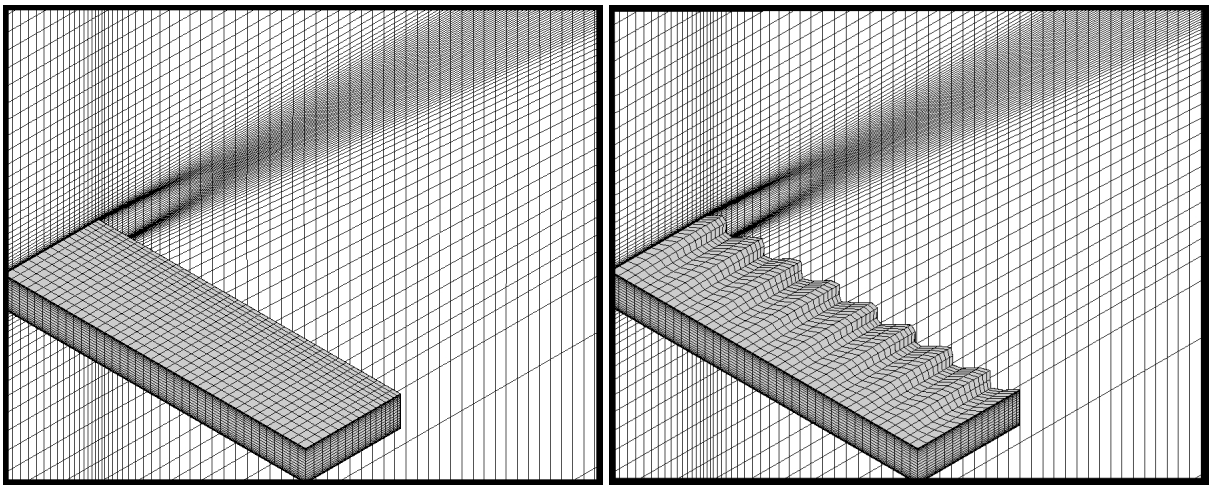

(a) Straight Edge (b) $\beta = 0.8$

Fig. 6 Curvilinear meshes used in the $\beta = 0$ and $\beta = 0.8$ simulations. Every 6th point has been shown for clarity. Care was taken to refine the mesh in zones near the splitter plate where boundary layers and shear layers develop.

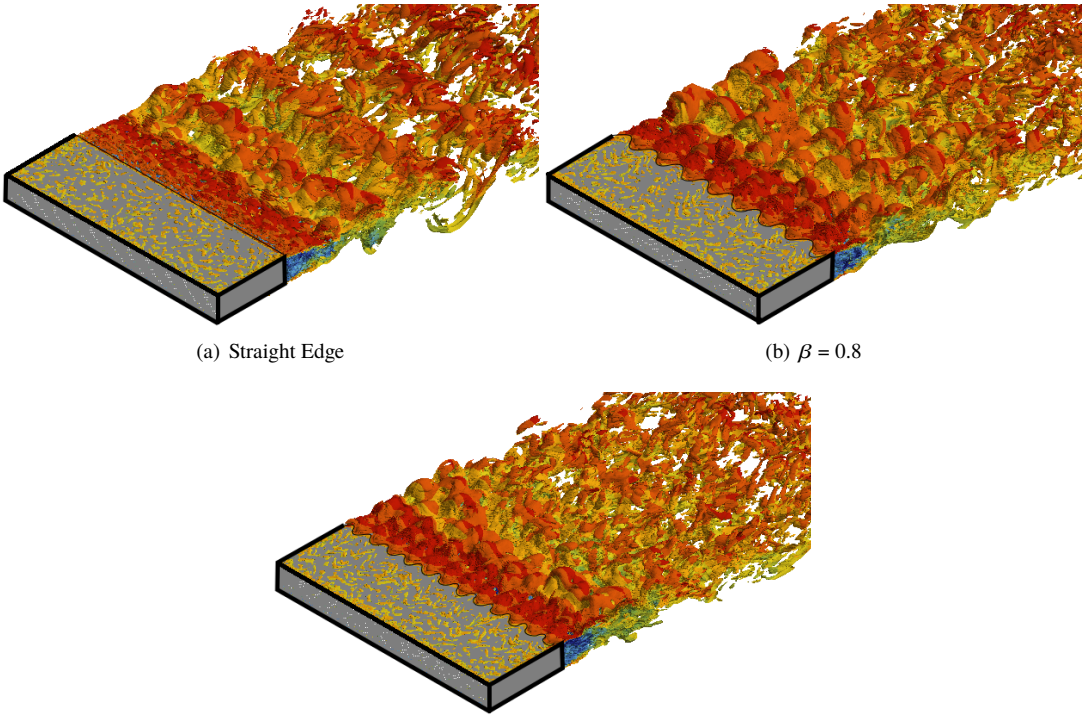

(a) Straight Edge (b) $\beta = 0.8$

(c) $\beta = 1.2$

Fig. 7 Isosurfaces of Q-criterion for the three different cases, colored by streamwise velocity

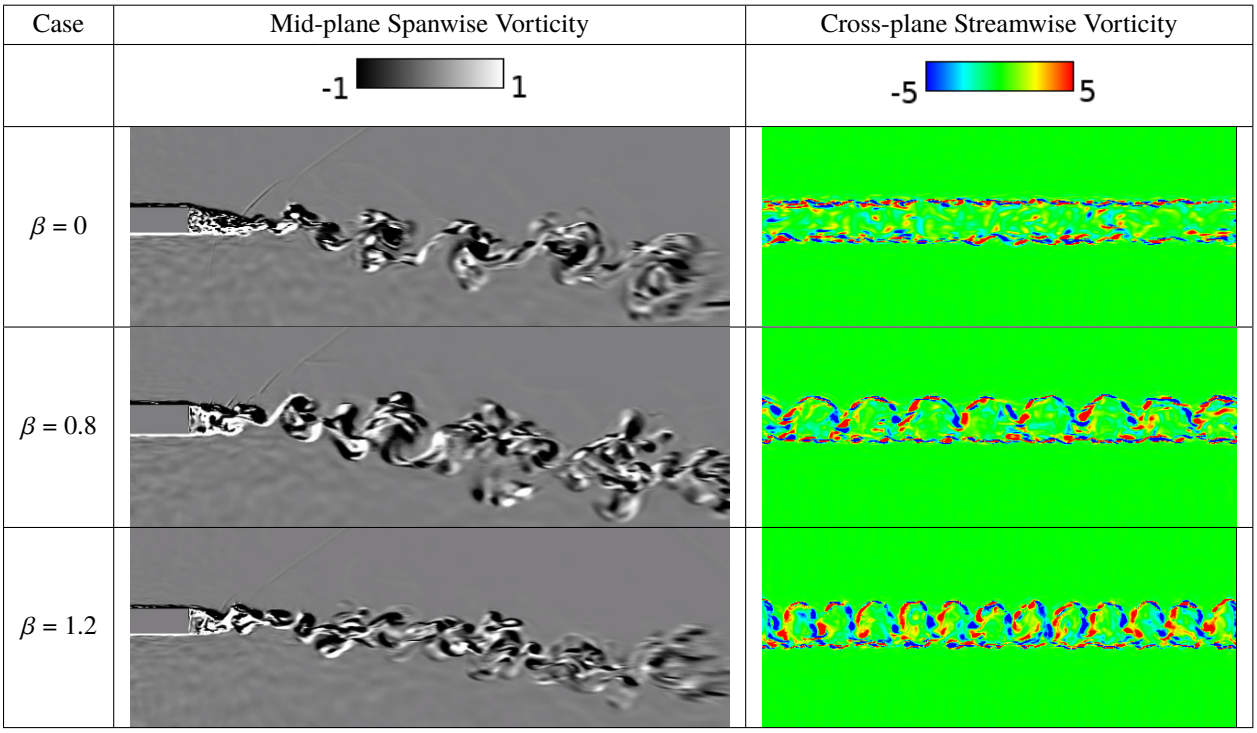

Fig. 8 Evolution of vorticity. Left: Gray scale representation of spanwise vorticity for the three cases. Right: Streamwise vorticity on cross-plane

between the two merging streams, as previously observed by Ruscher *et al* [20] and Stack *et al* [19]. It is clear however, that only the clockwise rotating vortices (when viewing the flow going from left to right) dominate far enough away from the SPTE. The counter-clockwise vortices, of the same sign as that in the lower separating boundary layer, are smaller in size and do not persist very far. The clockwise vorticity in the faster upper (core) boundary layer is larger, and is also consistent with the velocity gradient between the two streams, and thus dominates downstream. Stack *et al* [19] observed that the counter-clockwise vortices are suppressed in the full nozzle configuration due to the dissipative influence of the deck, however, Fig.7 and Fig.8 indicate that a deck plate is not necessary for a similar observation.

Plots of streamwise and spanwise vorticity shown in Fig.8. The individual vorticity components are plotted on two planes: one parallel to the freestream and cutting through the center of the plate for the spanwise component of vorticity, and the other cutting normal to the freestream at a distance of one splitter plate thickness away from the SPTE. The convecting structures in the straight edge case display a downward trajectory into the deck stream in all cases. This is due to both density and pressure differences, with the density of the core stream being higher than that of the deck stream. The effect of the former on deflecting shear layers has been examined by Bretonnet *et al* [29] in cases where the density gradient incurs mass diffusion phenomena. Overall, the net effect of higher pressure and density of the core stream is to generate a transverse velocity component directed towards the deck stream, which manifests as a deflection of the shear layer.

The $\beta = 0.8$ and $\beta = 1.2$ cases (Fig.7) show significant differences in coherent structures from the straight edge case. The ridges at the SPTE for these cases generate streamwise vortical structures which rapidly decay downstream and ultimately help enhance the breakdown of the spanwise coherent structures. This effect is greater for the larger $\beta = 1.2$ case than the $\beta = 0.8$ case *i.e.,* the plate with the larger number of undulations per unit length shows quicker breakdown of structures. The spanwise vorticity plots (Fig.8) show that in the $\beta = 0.8$ case, the coherent vortex structures present in the straight edge case have fragmented into fine-scaled structures. The $\beta = 1.2$ case further enhances this fragmentation and the large vortices seen in the straight-edge case are not evident. The braid region effectively diminishes with β, and is not perceptible in the β=1.2 case.

The streamwise vorticity plots (Fig.8) clarify this picture further. For the non-zero β cases, movement of fluid from the core stream to the deck stream starts earlier along the SPTE in the valleys, which later manifest as a vortex pair

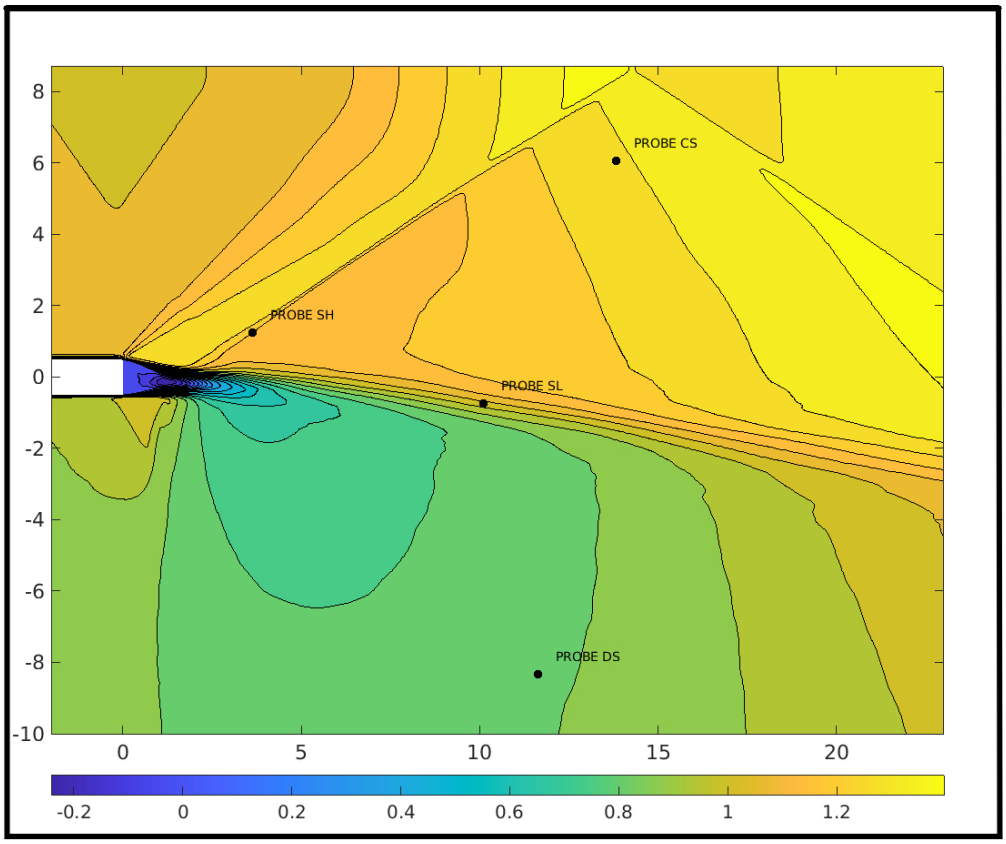

(a)

Fig. 9 Point probe locations for the spectral analysis. The plot shows time-averaged streamwise velocity for the straight-edge cases

inside each. The dissimilarity in the freestream conditions of the core and deck streams also indicates that the core stream side vortices entrain fluid faster and are thus more pronounced than the vortices on the deck stream side. This is consistent with the observation that the lobes in the streamwise vorticity plot are more curved along the core stream side of the flow.

To examine the impact of the SPTE on the frequency spectrum of the flow, we consider the temporal variation of pressure at the four locations shown in Fig.9. The probes record variations in four distinct regions of the flow, namely the primary shock, the shear layer, the core stream and the deck stream. The time-step-size used in the LES allows for a sampling rate of about 206MHz. After reaching statistical stationarity, the flow was marched through a minimum of 34000 time steps. The FFT spectra computed in this fashion are shown in Fig.10. A clear peak is visible at all four probe locations for the straight-edge case ($\beta = 0$), and occurs at a frequency of approximately 30 kHz. This value corresponds to that at which vortices are shed from the trailing edge of the splitter plate, and is in good agreement with the experiments [13] and simulations [18], where a similar tone was observed. The frequency signature of this shedding is most pronounced along the primary shock wave and the shear layer, due to the disturbance waves associated with the creation and passage of the vortices. This correlation between the unsteadiness associated with the vortices and propagation along the shock wave effectively permeates this frequency into the entire flowfield. The 30kHz peak is much smaller in the core and deck stream probes because these points are only indirectly affected by pressure waves propagating from the SPTE region and the formed vortices.

The spectral content of the probes for the $\beta = 0.8$ and $\beta = 1.2$ reveals that changing the SPTE geometry has significantly reduced the size of the 30kHz peak. This is consistent with the breakdown of coherent structures evident in Fig.7 and the left side of Fig.8. Clearly, the introduction of streamwise vorticity (right side of Fig. 8 enhances the breakdown of the spanwise vortex structures to yield a more broadband spectrum of frequencies with no distinct peaks.

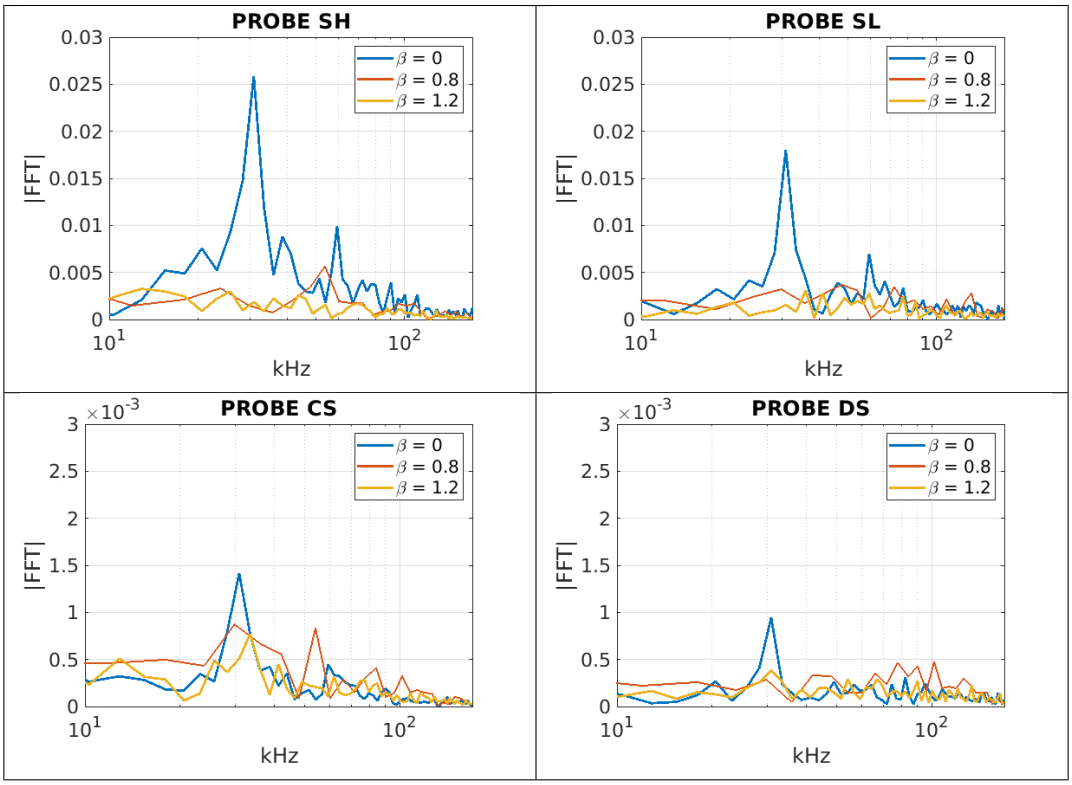

Fig. 10 Spectral content of the point probes for all three cases

This cannot be conclusively said about the spectrum of the probe on the shock however, since as described later, the introduction of a spanwise wavenumber alters the positions of the shocks.

The time-averaged mean of the straight-edge splitter plate case (Fig.9) reveals information about the growth of the shear layer that distinguishes it from that of a simple compressible shear layer. Initially, the core stream expands over the SPTE due to the increase in flow area that comes with the wake of the splitter plate. It then encounters the deck stream, which necessitates a change in flow direction, resulting in an oblique shock in the supersonic core stream. This shock reflects from the top boundary of the computational domain, which is modeled as an inviscid wall, and interacts with the shear layer at a downstream location outside of the region of interest. The downward deflection of the mixing layer generates a gradual expansion, observed above the shear layer of Fig. 9. This is accompanied by an acceleration of the upper stream, even as it entrains fluid from the lower speed stream below.

The flow of the sonic deck stream is also complex. Just before the SPTE, the deck stream also experiences an expansion (milder than that of the core stream) due to the sudden increase in flow area in the wake of the splitter plate. The deck stream also accelerates gradually along the streamwise direction, as it is inherently being driven by the high speed core stream through the action of shear. Although a compression is also observed by the deck stream, no distinct shock waves are seen in the time-averaged mean. Unsteady simulations however, have shown the distinct presence of weak compression waves propagating into the deck stream from the SPTE.

The evolution of the shear layer is correlated with changes in the vorticity thickness in the downstream direction [30]. An estimate of this phenomenon may be obtained by examining the variation of the maximum value of the reciprocal of $\partial u/\partial y$ with streamwise distance. This quantity is shown in Fig.11.a for all cases. In each case, the value downstream of the initial mean bubble ($x \simeq 2.5$) increases somewhat linearly but is subsequently characterized by non-linear growth and oscillatory behavior with a general upward trend. This is an interesting consequence of the difference in the properties of the two streams. The value of this variable increases monotonically in a simple mixing shear layer, where the external velocities of each stream remain constant. In the present case however, the presence of the gradual expansion downstream of the primary shock marked in Fig. 9, and the shear layer deflection, has the effect of altering the effective freestream velocity of each stream. The value of $1/(\partial u/\partial y)$ is thus not monotonic in any of the curves of Fig. 11.a).

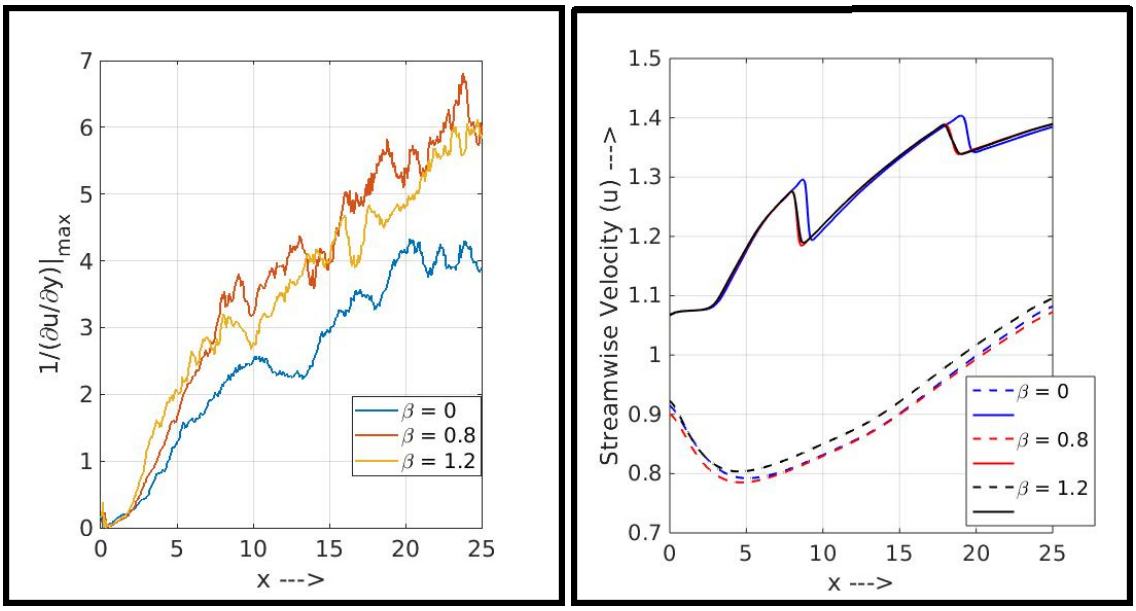

(a) (b)

Fig. 11 a)Non-linear growth of the shear layer for the three cases, visualized through the value of the reciprocal of largest value of $\partial u/\partial y$ along a vertical line. b)Streamwise plot of the freestream velocities for all three cases. The velocities were computed at a vertical distance of 5 splitter plate thicknesses above and below the center of the splitter plate. The solid lines are for the core stream and the dotted lines are for the deck stream. In both plots a) and b) the coordinate x = 0 corresponds to the tip of the SPTE

Fig.11.a also shows that the non-zero β cases enhance the growth of the shear layer throughout its length.

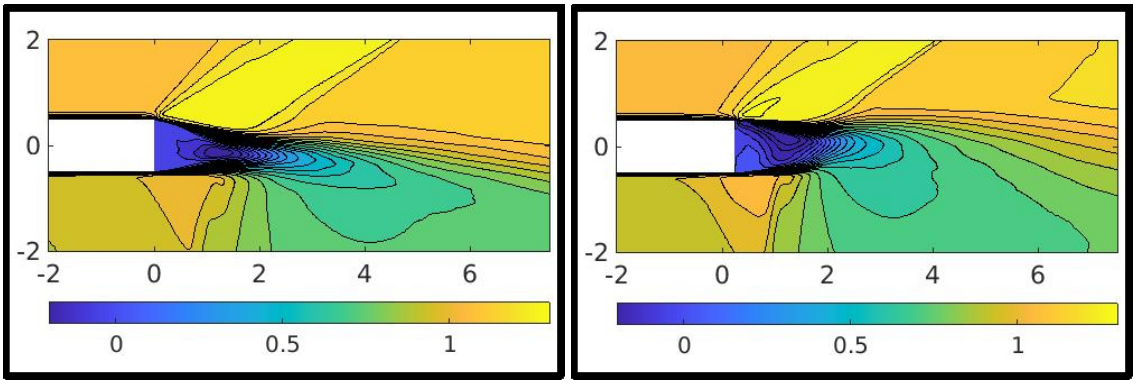

(a) Straight Edge (b) $\beta = 0.8$

Fig. 12 Shear layer curvature visualized using time-averaged streamwise velocity plots

The effect of the SPTE geometry on the freestream velocities is shown in Fig.11.b). In the streamwise direction, for the non-zero β cases, the locations of the primary and reflected shocks are upstream of those for the baseline case. This is due to the fact that the relief effect of the valley regions allow the core and deck streams to interact slightly earlier than the $\beta = 0$ case. A secondary consequence of this is that the shear layer develops an upward curvature near the SPTE. This is more clearly evident in Fig.12, which plots the streamwise velocity contours in the region near the SPTE. The particular location for the $\beta = 0.8$ case is chosen so that the edge is locally at a similar streamwise location as the baseline. The upward curvature can be explained by the fact that for the non-zero β cases, the enhanced streamwise

vorticity induced by the ridges and valleys increases the mixing between the two streams. This mixing enhancement is not only proportional to the wavenumber used, but is also strongly affected by the amplitude of the spanwise features of the SPTE geometry. Thus, a larger amplitude, with deeper ridges and valleys, encourages mixing and changes the size and shape of the recirculation bubble that is formed in front of the SPTE. This change is visible in Fig.12 where the recirculation bubble in the straight-edge case appears long and narrow, while the $\beta = 0.8$ case displays a shorter but vertically broader bubble. The difference in the bubble shape leads to a smaller distance through which the core stream can expand before the primary oblique shock. Thus, the shear layer appears to curve slightly upward. However, downstream of the bubble, the freestream differences between the two layers are the dominant influence, and the shear layer once again curves down toward the deck stream. As noted earlier, the above computational results are being used to inform the experimental thrust of the program. To this end, Fig. 13 displays the CAD file of splitter plate being currently machined for subsequent use in the experimental SERN facility at Syracuse University.

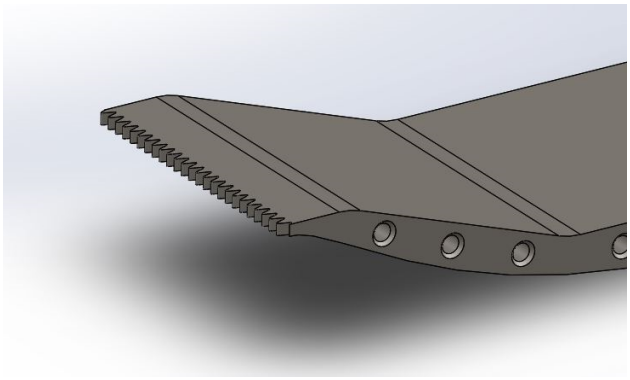

Fig. 13 CAD file for the machined plate for $\beta = 0.8$.

IV. Effect of Aft-Deck Length

The second component of the effort to examine the effect of varying the configuration considers the deck length, which can have a significant impact on the plume. In addition to the nominal deck length employed in the original design [13, 21], results are now described for half and double lengths, as well as for the case where the deck is removed. Unlike the simulation thrust above, which sought to isolate the effect of the SPTE, deck length studies are necessarily conducted in the actual MARS configuration *i.e.,* including the SERN.

A. Experimental Approach

The effects of geometric modifications of the aft-deck and splitter plate on the flow physics is explored through simultaneous measurements of the velocity field, and pressures obtained in the anechoic chamber, shown in Fig.14.

Three diagnostic techniques are used in the examination of the MARS in the Skytop Turbulence Laboratory at Syracuse University. This campaign uses Particle Image Velocimetry (PIV), a far-field microphone array, and near-field dynamic pressure transducers. PIV uses tracer particles, together with an optical technique, to visualize the flow and determine the velocity field. Two consecutive laser pulses illuminate the tracer particles. Stereoscopic PIV captures the locations of the particles simultaneously with two cameras at different viewing angles, which facilitates the extraction of the three velocity components on a two-dimensional plane. The cameras, laser, and sheet optics are mounted on a two-axis traverse to allow for tests of multiple planes in the streamwise and cross-stream directions.

Fig. 15 provides a visualization of the planes. Plane locations are normalized by the hydraulic diameter, defined by:

$$D_h = \frac{2h_e w}{h_e + w} \tag{4}$$

For the current configuration, D_h is $44.5mm$. Streamwise measurements are performed for z/D_h = -1, 0, 0.25, 0.5, 0.75, 1 and cross-stream x/D_h = 4, 5, 6, 7, 8. Additional planes may be explored to provide overlapping statistics. PIV contour maps of the extended deck plate are provided and discussed in Section IV.B.

In addition to flow visualization, pressure measurements are obtained through far-field microphones and near-field pressure transducers. A horizontal in-plane array is used to sample the acoustics in the far-field of the jet nozzle exit, as

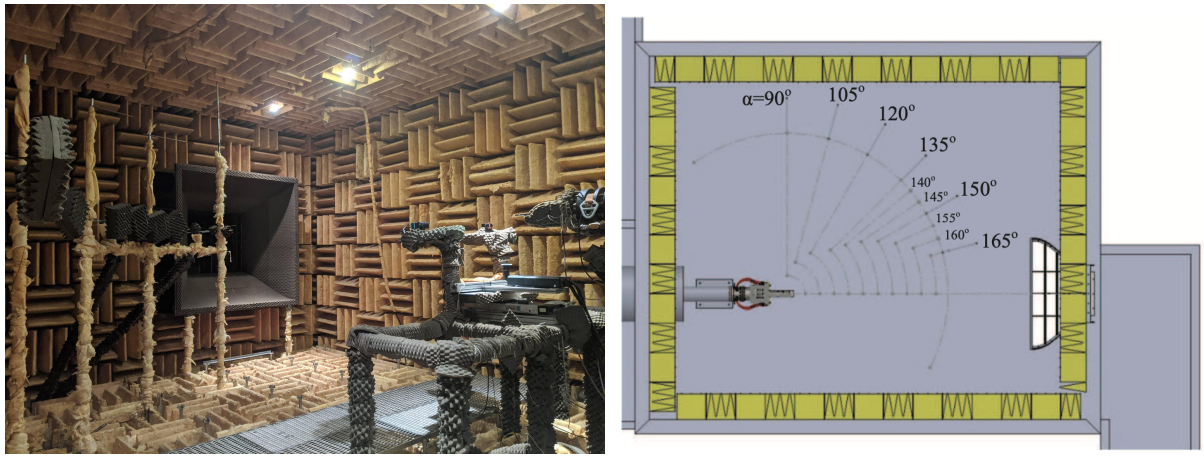

(a) Anechoic Chamber (b) Microphone Array Schematic

Fig. 14 a) Experimental setup in anechoic chamber. b) Schematic of microphone array locations in reference to nozzle exit.

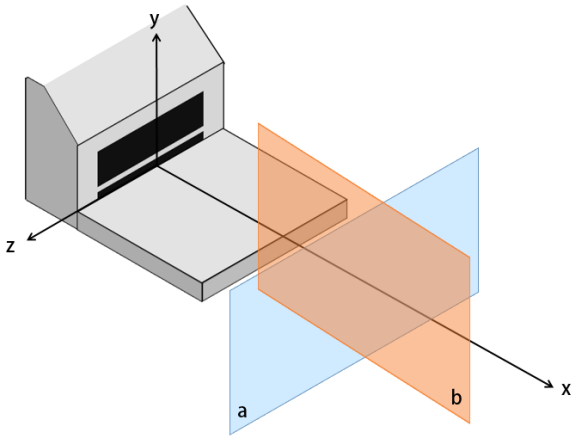

Fig. 15 A schematic of the planes for PIV. a) Cross-stream, b) Streamwise.

shown in Fig. 14. The 10 microphones are mounted on the circular array spaced from 90° to 135° in steps of 15° and increments of 5° from 135° to 165°, as shown in Fig. 14 b., to provide higher resolution. In addition to the far-field sensors, transducers are fitted to the nominal length polycarbonate aft-deck plate to provide insight as to how changes in the instability could affect the unsteady loading on the deck plate. The transparency of the polycarbonate allows for the simultaneous capture of pressure measurements and PIV closer to the nozzle exit with minimal wall reflections.

As seen in Fig.3, the splitter plate resides within the steel jet and is not easily accessible. The ability to integrate hardware into the splitter plate to capture measurements such as fluctuating pressure is limited by the thickness of the SPTE which is approximately three millimeters. Since it is difficult to introduce probes into the jet, the measurements are restricted to the near-field of the nozzle exit (the aft-deck plate). For flow visualization of the region, PIV and LDA were considered. The former is not suitable to capture the events inside the current jet rig because of the steel walls. LDA is also unsuitable because of reflections in the narrow space. This difficulty points to the need for the ongoing computational component; the experimental results below are guiding an ongoing LES campaign addressing the full configuration, as a continuation of the work of Ref. [21]. This complementary effort should help completely characterize the effects of spanwise geometry alterations on the instability throughout the entire domain.

B. Results

The following results further the exploration of deck length modifications, a continuation of the efforts in Ref. [16], for the nominal splitter plate. PIV results were obtained for the MARS jet with the original splitter plate and an aft-deck of $4D_h$. Tests were run at design conditions of $M_{j,1}$ = 1.6 and $M_{j,3}$ = 1.0 to match those performed by Berry [16]. The nozzle was heated to approximately 180° F to remove vapor cloud formation for PIV experiments. While performing tests, it was noted that the end of the deck plate experienced small vibrations due to the unsteady loading causing the end of the deck to deflect a maximum of 1 mm.

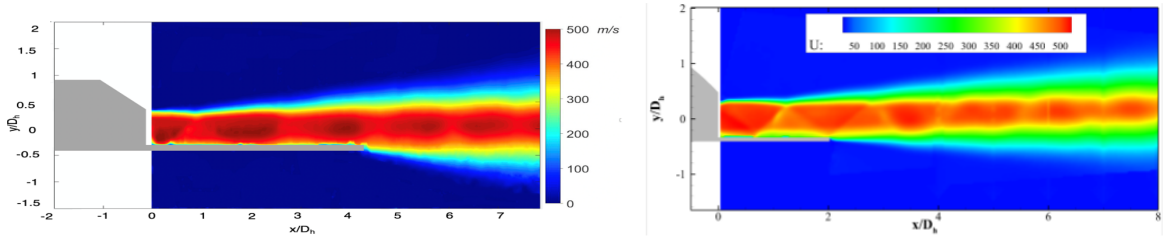

(a) Twice Nominal

(b) Nominal

(c) Half Nominal

(d) No Deck

Fig. 16 Time averaged u-component of velocity taken at z/D_h = 0.

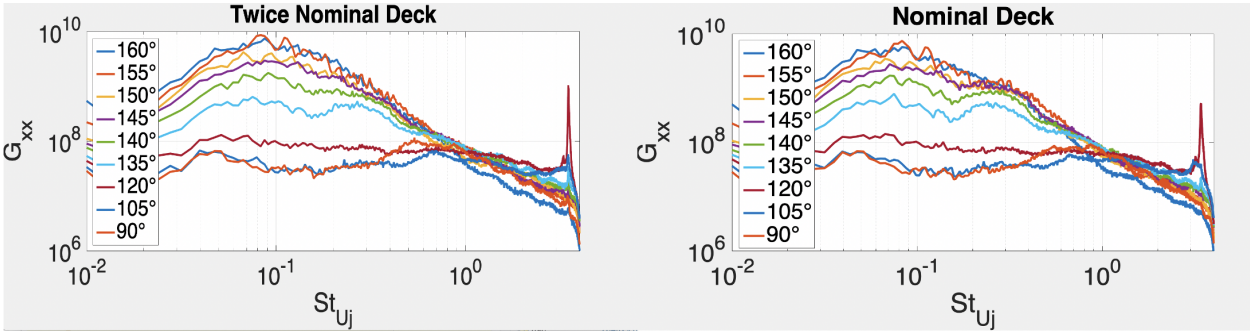

Fig. 17 One-sided auto spectral density of twice nominal and nominal deck.

The time averaged u-component of velocity contours for the no deck, half deck, nominal and twice nominal lengths at the streamwise plane z/D_h = 0 are displayed in Fig. 16. These contours further show the ability to experimentally analyze the flow field as originally shown by Berry [16]. Initial observations of the extended deck show the jet plume deflecting minimally downward. A slight separation region is evident at the trailing edge, beginning roughly at x/D_h = 3.5, with an associated shock, more closely resembling the half deck results. Differences in jet plume deflection of the deck cases shows agreement with the work of Ref. [25], who demonstrated that the shock train at the trailing edge, and subsequent plume deflection, could be altered by adjusting the NPR and/or aft-deck length [25]. Additionally, the apparent reattachment and second separation just before the trailing edge affects the shock motion, and potentially interacts with the vibration of the deck at certain times during the run. This phenomenon warrants additional

investigation.

This analysis coincides with the optimized deck geometry shown by [31]. Figure 17 displays the autospectral density for the nominal and twice nominal cases. Data for two of the microphones were neglected due to inoperable devices. Examination of the overall sound pressure levels for this modified geometry show a slight reduction to the nominal case from 99.35 dB to 98.27 dB. Further measurements at various operating conditions are yet to be explored for additional comparison of the effects of the extended deck length. The results will then be used to inform select LES cases.

V. Conclusion and Future Work

Two aspects of the design of rectangular multi-stream nozzles were examined. The first addressed the source of a tone, associated with the trailing edge of the splitter plate. For this, LES simulations were performed on three different splitter plates, of same dimensions as in the full nozzle configuration, but with a straight edge and spanwise wavenumbers of 0.8 and 1.2. This goal was to explore the effect of the spanwise wavenumber of the SPTE on the instability responsible for the tone. The non-zero β cases were successful in reducing the signature of the vortex-shedding, as evidenced by the spectra of point probes placed at different locations around the flow. Visualizations of the spanwise and streamwise vorticity revealed that the mechanism through which this was accomplished was the introduction of streamwise vortex structures that interfered with the natural formation of spanwise vortices in the shear layer. The breakdown of these structures results in incoherent turbulence that allow the two streams to mix faster. The SPTE geometry had unintended side-effects such as shifting the shock structure in the flow slightly upstream and changing the initial curvature of the shear layer. Spectrum from LES provides evidence that the dominating 30kHz observed in the far field of the nominal splitter plate case is not present in the sinusoidal SPTE case. Reduction of this tone may reveal more distinct variations in deck geometries and their subsequent effects on the flow physics. Several deck lengths (nominal, half-nominal, twice-nominal and no-deck) were also examined in the context of the full rectangular multi-stream nozzle designated MARS. The results show clear effect on the evolution of the downstream plume as well as the shear layer initiated at the deck trailing edge. The effect on the tone was modest, with a slight reduction in the sound level when the deck was extended. Future work will complete each campaign, and provide guidance for the complementary experiments to examine the wavy splitter plate inside the actual MARS configuration, and simulations on modified deck length which can better probe the observed behavior on the flow over the deck.

Acknowledgments

This study was provided funding by the Air Force Office of Scientific Research (AFOSR) grant number FA9550-19-1-0081, Dr. Gregg Abate, program manager. The authors would like to acknowledge Dr. Jacques Lewalle and Dr. Cory Stack, whose findings provided motivation for this investigation. Thanks to Dr. Christopher Ruscher of Spectral Energies LLC for discussions of this problem. Additionally, the authors would like to acknowledge Tyler Vartabedian for experimental support in the Skytop facility.

References

[1] Kyprianidis, K. G., "Multi-disciplinary conceptual design of future jet engine systems," 2010.

[2] De la Rosa Blanco, E., Hall, C., and Crichton, D., "Challenges in the silent aircraft engine design," *45th AIAA aerospace sciences meeting and exhibit*, 2007, p. 454.

[3] Meher-Homji, C. B., "The development of the Whittle turbojet," 1998.

[4] Koff, B. L., Budinger, R. E., and Johnson, J. E., "Modulating bypass variable cycle turbofan engine," , Mar. 28 1978. US Patent 4,080,785.

[5] Simmons, R. J., "Design and control of a variable geometry turbofan with and independently modulated third stream," Ph.D. thesis, The Ohio State University, 2009.

[6] CAPONE, F., "The nonaxisymmetric nozzle-It is for real< 149> fighter aircraft performance viewpoint," *Aircraft Systems and Technology Meeting*, 1979, p. 1810.

[7] Deere, K. A., and Asbury, S. C., "Experimental and Computational Investigation of a Translating-Throat Single-Expansion-Ramp Nozzle," 1999.

[8] Bruening, G. B., and Chang, W. S., "Cooled cooling air systems for turbine thermal management," *ASME Paper*, Vol. 14, 1999, p. V003T01A002.

[9] Papamoschou, D., and Debiasi, M., "Directional suppression of noise from a high-speed jet," *AIAA journal*, Vol. 39, No. 3, 2001, pp. 380–387.

[10] Magstadt, A., Berry, M., Shea, P., Glauser, M., Ruscher, C., Gogineni, S., and Kiel, B., "Aeroacoustic experiments on supersonic multi-aperture nozzles," *53rd AIAA/ASME/SAE/ASEE Joint Propulsion Conference*, Orlando, FL, 2015.

[11] Berry, M. G., Magstadt, A. S., Glauser, M. N., Ruscher, C. J., Gogineni, S. P., and Kiel, B. V., "An acoustic investigation of a supersonic, multi-stream jet with aft deck: Characterization and acoustically-optimal operating conditions," *54th AIAA Aerospace Sciences Meeting*, 2016, p. 1883.

[12] Johnson, J., "Variable cycle engine developments at General Electric 1955-1995," *Developments In High-Speed Vehicle Propulsion Systems*, 1995, pp. 105–158.

[13] Berry, M., Magstadt, A., and Glauser, M. N., "Application of POD on time-resolved schlieren in supersonic multi-stream rectangular jets," *Physics of Fluids*, Vol. 29, No. 2, 2017, p. 020706.

[14] Berry, M. G., Stack, C. M., Magstadt, A. S., Ali, M. Y., Gaitonde, D. V., and Glauser, M. N., "Low-dimensional and data fusion techniques applied to a supersonic multistream single expansion ramp nozzle," *Physical Review Fluids*, Vol. 2, No. 10, 2017, p. 100504.

[15] Berry, M. G., Stack, C. M., Magstadt, A., Gaitonde, D., and Glauser, M., "Analysis of a rectangular supersonic multi-stream jet by LES and experiments," *Turbulence and Shear Flow Phenomena*, Vol. 10, 2017.

[16] Berry, M. G., "Investigating the Interaction of a Supersonic Single Expansion Ramp Nozzle and Sonic Wall Jet," Ph.D. thesis, Syracuse University, 2016.

[17] Magstadt, A. S., "Investigating the Structures of Turbulence in a Multi-Stream, Rectangular, Supersonic Jet," Ph.D. thesis, Syracuse University, 2017.

[18] Stack, C. M., and Gaitonde, D. V., "Shear Layer Dynamics in a Supersonic Rectangular Multistream Nozzle with an Aft-Deck," *AIAA Journal*, Vol. 56, No. 11, 2018, pp. 4348–4360.

[19] Stack, C. M., "Turbulence Mechanisms in a Supersonic Rectangular Multistream Jet with an Aft-Deck," Ph.D. thesis, The Ohio State University, 2019.

[20] Ruscher, C. J., Gogineni, S., and Ferrill, T., "Splitter Plate Edge Effects in a Supersonic Multi-stream Nozzle," *2018 Joint Propulsion Conference*, 2018, p. 4745.

[21] Stack, C. M., and Gaitonde, D. V., "Mechanisms Influencing Surface Pressure Unsteadiness on the Aft-Deck of a Rectangular Multistream Supersonic Nozzle," *2018 AIAA Aerospace Sciences Meeting*, 2018, p. 0822.

[22] Gerrard, J., "The mechanics of the formation region of vortices behind bluff bodies," *Journal of fluid mechanics*, Vol. 25, No. 2, 1966, pp. 401–413.

[23] Fernando, E., and Menon, S., "Mixing enhancement in compressible mixing layers-An experimental study," *AIAA journal*, Vol. 31, No. 2, 1993, pp. 278–285.

[24] Lewalle, J., Stack, C., Ruscher, C. J., and Gogineni, S., "Regions of anomalous acoustic propagation in a complex supersonic jet*," *2020 AIAA Aerospace Sciences Meeting*, 2020.

[25] Stack, C. M., Gaitonde, D. V., Agostini, L., Berry, M. G., Magstadt, A. S., and Glauser, M. N., "Numerical investigation of a supersonic multistream jet with an aft-deck," *54th AIAA Aerospace Sciences Meeting, 2016*, American Institute of Aeronautics and Astronautics Inc, AIAA, 2016.

[26] Adler, M. C., Gonzalez, D. R., Stack, C. M., and Gaitonde, D. V., "Synthetic generation of equilibrium boundary layer turbulence from modeled statistics," *Computers & Fluids*, Vol. 165, 2018, pp. 127–143.

[27] Roe, P. L., "Approximate Riemann solvers, parameter vectors, and difference schemes," *Journal of computational physics*, Vol. 43, No. 2, 1981, pp. 357–372.

[28] Van Leer, B., "Towards the ultimate conservative difference scheme. V. A second-order sequel to Godunov's method," *Journal of computational Physics*, Vol. 32, No. 1, 1979, pp. 101–136.

[29] Bretonnet, L., Cazalbou, J.-B., Chassaing, P., and Braza, M., "Deflection, drift, and advective growth in variable-density, laminar mixing layers," *Physics of Fluids*, Vol. 19, No. 10, 2007, p. 103601.

[30] Freeman, J. L., "On the growth rate of turbulent mixing layers: A new parametric model," 2014.

[31] DiDominic, D., Gist, E., Fitzgerald, J., and Glauser, M. N., "Complex Nozzle Optimization Techniques using Machine Learning," *AIAA Scitech 2020 Forum*, 2020, p. 1866.